Bioorganic & Medicinal Chemistry 20 (2012) 2444–2454

Contents lists available at SciVerse ScienceDirect

Bioorganic & Medicinal Chemistry

journal homepage: www.elsevier.com/locate/bmc

N^4-(3-Bromophenyl)-7-(substituted benzyl) pyrrolo[2,3-*d*]pyrimidines as potent multiple receptor tyrosine kinase inhibitors: Design, synthesis, and in vivo evaluation

Aleem Gangjee [a,*], Nilesh Zaware [a], Sudhir Raghavan [a], Jie Yang [a], Jessica E. Thorpe [b], Michael A. Ihnat [b]

[a] Division of Medicinal Chemistry, Graduate School of Pharmaceutical Sciences, Duquesne University, 600 Forbes Avenue, Pittsburgh, PA 15282, USA
[b] Department of Cell Biology, School of Medicine, University of Oklahoma Health Sciences Center, Oklahoma City, OK 73104, USA

ARTICLE INFO

Article history:
Received 16 September 2011
Revised 11 January 2012
Accepted 19 January 2012
Available online 4 February 2012

Keywords:
Multiple receptor
Tyrosine kinase inhibitors
Antiangiogenic agents

ABSTRACT

With the goal of developing multitargeted receptor tyrosine kinase inhibitors that display potent inhibition against PDGFRβ and VEGFR-2 we designed and synthesized eleven N^4-(3-bromophenyl)-7-(substitutedbenzyl) pyrrolo[2,3-*d*]pyrimidines **9a**–**19a**. These compounds were obtained from the key intermediate N^4-(3-bromophenyl)-7*H*-pyrrolo[2,3-*d*]pyrimidine-2,4-diamine **29**. Various arylmethyl groups were regiospecifically attached at the N7 of **29** via sodium hydride induced alkylation with substituted arylmethyl halides. Compounds **11a** and **19a** were potent dual inhibitors of PDGFRβ and VEGFR-2. In a COLO-205, in vivo tumor mouse model **11a** demonstrated inhibition of tumor growth, metastasis, and tumor angiogenesis that was better than or comparable to the standard compound TSU-68 (SU6668, **8**).

1. Introduction

Protein kinases are enzymes that transfer a phosphate group from ATP to the hydroxyl group of serine, threonine, or tyrosine of specific proteins inside cells.[1] The phosphorylation by these enzymes achieves an important function of signal transduction in eukaryotic cells and controls the processes of cell proliferation, metabolism, survival, and apoptosis. A mis-regulation of these tightly controlled processes results in the overexpression of kinases, which is associated with a variety of disease states including cancer.[2]

Angiogenesis is the process of formation of new blood vessels from existing vascular bed. Angiogenesis is crucial for a tumor to grow beyond 1–2 mm and for tumor invasion and metastasis.[3,4] As a tumor grows in size, it becomes increasingly hypoxic and triggers the release of growth factors, particularly, vascular endothelial growth factor (VEGF), epidermal growth factor (EGF), and platelet derived growth factor (PDGF) among others. The growth factors activate adjacent blood vessels leading to angiogenesis.[5,6] Following angiogenesis, the tumor can grow at an increased rate.[7]

For angiogenesis to occur, the pro-angiogenic growth factors have to bind to members of the protein kinase family identified as receptor tyrosine kinases (RTKs). Following binding, the RTKs dimerize and undergo autophosphorylation, initiating a series of downstream events leading to proliferation migration and cell survival.[8] The growth factor VEGF triggers angiogenesis by binding to a family of VEGF receptors, including VEGFR-2 (KDR), VEGFR-1 (Flt-1), and VEGFR-3 (Flt-4). Similarly PDGF binds to the family of PDGF receptors, Flt-3 (FMS-like tyrosine kinase-3), PDGFRβ, c-Kit (a stem cell factor receptor), and CSF1R (colony-stimulating factor 1 receptor).[9]

Abrogation of angiogenesis by inhibition of RTK signaling pathways is an important mechanism for the development of novel anticancer agents.[8,10,11] Early work in the area of RTK inhibitor discovery afforded small molecule inhibitors gefitinib **1** (Fig. 1) (specific EGFR inhibitor, approved for limited use for the treatment of non-small cell lung cancer)[12] and erlotinib **2** (specific EGFR inhibitor, approved for the treatment of non-small cell lung cancer).[12] Recent data, however, shows that tumors treated with specific RTK inhibitors usually develop resistance through the upregulation of alternate kinase mediated pathways.[13] In addition, cross-talk has been implicated between EGFR and other growth factor receptors involved in tumor development.[14]

Abbreviations: ATP, adenosine 5′triphosphate; VEGF, vascular endothelial growth factor; EGF, epidermal growth factor; PDGF, platelet derived growth factor; RTK, receptor tyrosine kinase; KDR, kinase insert domain receptor; VEGFR-2, vascular endothelial growth factor receptor-2; Flt-1, fms-related tyrosine kinase 4; VEGFR-1, vascular endothelial growth factor receptor-1; Flt-4, fms-related tyrosine kinase 4; VEGFR-3, vascular endothelial growth factor receptor-3; Flt-3, FMS-like tyrosine kinase-3; PDGFRβ, platelet derived growth factor receptor-β; CSF1R, colony stimulating factor 1 receptor; CML, chronic myelogenous leukemia; GIST, gastrointestinal stromal tumor; Abl, abelson tyrosine kinase; ErbB-2, erythroblastic leukemia viral oncogene homolog-2; TLC, thin layer chromatography; CAM, chorioallantoic membrane.

* Corresponding author. Tel.: +1 412 396 6070; fax: +1 412 396 5593.
E-mail address: gangjee@duq.edu (A. Gangjee).

0968-0896/$ - see front matter © 2012 Elsevier Ltd. All rights reserved.
doi:10.1016/j.bmc.2012.01.029

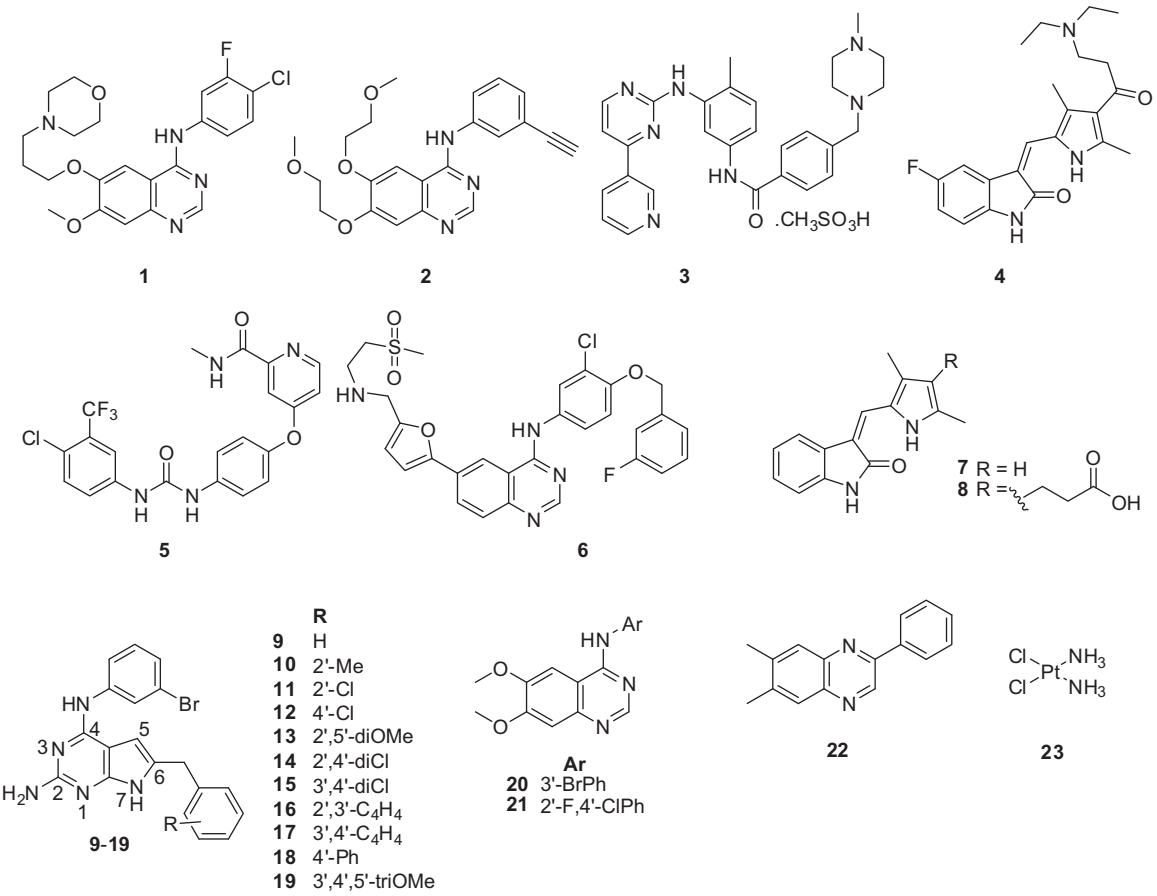

Figure 1. RTK Inhibitors.

There are a number of RTK mediated processes that can promote angiogenesis, thus inhibitors targeting a broader range of RTKs may lead to a more robust antitumor response and prevent resistance by targeting two or more angiogenic pathways.[15,16] The FDA approval of several compounds targeting a broader-spectrum of RTKs lends credence to the development of single agents that target multiple RTKs. These include imatinib **3**, sunitinib **4**, sorafenib **5** and lapatinib **6** (Fig. 1). Compound **3** inhibits Abelson Tyrosine Kinase (Abl), c-kit protein (CD117), and PDGFR, and has been approved for chronic myelogenous leukemia (CML),[17] gastrointestinal stromal tumors (GISTs), and other malignancies. Compound **4** inhibits VEGFR-2, PDGFRβ, c-kit, and FMS-like tyrosine kinase 3 (FLT3)[18] and has been approved for the treatment of renal cell carcinoma and imatinib-resistant GIST. Compound **5** inhibits Raf kinase, VEGFR-2, PDGFRβ, and c-kit[19] and has been approved for advanced renal cell carcinoma. Compound **6** inhibits EGFR and erythroblastic leukemia viral oncogene homolog-2 (ErbB-2)[20] and has been approved for advanced metastatic breast cancer in conjunction with chemotherapy.

In angiogenesis, VEGFs cause a significant increase in the formation of blood vessels, but these vessels are immature and leaky. The formation of thicker, more stable vessels requires an encapsulation by pericytes. This process of encapsulation is driven by PDGFRβ signaling. Recent reports indicate that the inhibition of VEGFR-2 and PDGFRβ with two separate inhibitors produces a synergistic effect in early stage as well as late stage pancreatic islet cancer in mouse models.[21] Timke et al.[22] have investigated the therapeutic potential of a VEGFR inhibitor SU5416 (**7**) (Fig. 1) and PDGFR inhibitor **8**[23,24] in combination with radiotherapy in vitro and in vivo. It was observed that dual inhibition of VEGFR and PDGFR signaling was a more efficient antitumor mechanism than single pathway inhibition. In addition radiation markedly enhanced the therapeutic efficacy in vitro and in human glioblastoma and human prostrate carcinoma in mice.

We[25] previously reported a series of eleven N^4-(3-bromophenyl)-6-(substituted benzyl) pyrrolo[2,3-*d*] pyrimidines **9**–**19** (Fig. 1). These compounds were evaluated in human tumor cells known to over express high levels of specific RTKs. Compound **10** with a 2′-Me benzyl substitution exhibited toxicity against A431 cells (cell lines overtly dependent on EGFR for survival)[26] at values 10-fold better than the standard agent PD153035 (**20**) used in this assay (Table 1). In addition, **10** also demonstrated VEGFR-2 inhibition 40-fold better than the standard agent **7**. EGFR and A431 cell lines were inhibited by **14** (with a 2′,4′-diCl benzyl substitution) at concentrations that were comparable to and fivefold better than the standard **20**, respectively. Compound **13** with a 2′,5′-diOMe benzyl substitution inhibited VEGFR-2 and PDGFRβ at values 17-fold better than, and comparable to, standard agents **23** and AG1295 (**22**), respectively. Thus the N^4-(3-bromophenyl)-6-(substituted benzyl) pyrrolo[2,3-*d*]pyrimidine scaffold with variations in the phenyl ring affords multi-kinase inhibition with potencies equivalent to or better than standard agents. In an attempt to develop compounds with multikinase inhibition potential it was of interest to explore the effect of moving the 6-position substituent in the parent compounds to the 7-position. Hence a series of N^4-(3-bromophenyl)-7-(substituted benzyl) pyrrolo[2,3-*d*]pyrimidines—**9a**–**19a** (Fig. 2) was designed. The selection of the substituents on the N7-position is the same as that at N6 in the parent series (**9**–**19**), and is rationalized below.

Compound **9a** (Fig. 2) with a benzyl at N7 served as a comparison with compounds **10a** to **19a** (Fig. 2) that possess varied substituents at the N7 position. The basis for including the 2′-Me

Table 1
IC_{50} values (μM) of kinase inhibition and the A431 cytotoxicity assay

Compd #	PDGFR-β inhibition	VEGFR-2 inhibition	VEGFR-1 inhibition	EGFR inhibition	A431 cytotoxicity
9[a]	>50	>50	>50	1.67 ± 0.3	31.8 ± 6.3
10[a]	>50	0.25 ± 0.04	>50	9.19 ± 1.8	1.21 ± 0.42
11[a]	>50	5.58 ± 0.69	26.8 ± 4.1	4.31 ± 1.75	>50
12[a]	>50	8.28 ± 0.69	42.7 ± 6.1	17.42 ± 3.9	28.6 ± 5.1
13[a]	8.92 ± 1.6	0.62 ± 0.21	31.1 ± 5.8	12.62 ± 3.3	>50
14[a]	17.0 ± 5.6	28.11 ± 9.9	>50	0.23 ± 0.06	2.8 ± 1.1
15[a]	>50	>50	>50	19.77 ± 5.6	33.5 ± 6.2
16[a]	>50	5.08 ± 0.83	19.2 ± 4.3	>50	>50
17[a]	>50	>50	15.2 ± 2.9	1.24 ± 0.21	33.2 ± 5.9
18[a]	>50	5.97 ± 0.78	>50	6.16 ± 1.2	23.5 ± 5.2
19[a]	14.7 ± 3.4	9.42 ± 1.9	>50	>50	42.1 ± 18.5
9a	>500	23.8 ± 3.0	99.3 ± 10.3	166.4 ± 20.6	50.4 ± 5.9
10a	159.6 ± 26.3	113.4 ± 17	129.3 ± 20.4	113.3 ± 18.9	15.7 ± 2.8
11a	1.5 ± 0.21	17.9 ± 2.4	126.3 ± 19.1	>200	88.4 ± 10.2
12a	>500	65.3 ± 7.9	79.9 ± 8.4	99.9 ± 18.6	16.1 ± 2.2
13a		>200	>200	69.2 ± 6	40.6
14a	34.2 ± 4.4	>200	138.1 ± 24.2	>200	15.3 ± 1.9
15a	229.6 ± 37.1	64.5 ± 7.8	118.6 ± 11.4	>200	19.2 ± 3.0
16a	129.3 ± 21.1	14.9 ± 2.1	150 ± 22.1	>200	36.3 ± 4.9
17a	212.4 ± 16.2	22.9 ± 2.9	50.8 ± 6.2	>200	20.4 ± 3.5
18a	129.1 ± 20.5	22.9 ± 10.7	>200	>200	13.3 ± 20.5
19a	1.8 ± 0.29	25.7 ± 4.6	156.5 ± 25	>200	39.0 ± 6.8
20				0.2 ± 0.04	12.6 ± 2.9
21			17.7 ± 5.5		
7		2.43 ± 0.32			19.2 ± 1.1
22	6.2 ± 1.3				
23		10.6 ± 3.5			

[a] IC_{50} values taken from Ref. 25.

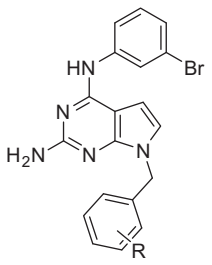

	R
9a	H
10a	2'-Me
11a	2'-Cl
12a	4'-Cl
13a	2',5'-diOMe
14a	2',4'-diCl
15a	3',4'-diCl
16a	2',3'-C_4H_4
17a	3',4'-C_4H_4
18a	4'-Ph
19a	3',4',5'-triOMe

Figure 2. Target compounds.

benzyl group in **10a**, 2′,5′-diOMe benzyl group in **13a**, and 2′,4′-diCl benzyl group in **14a**, was the potent RTK inhibition produced by the lead compounds **10**, **13**, and **14** (Fig. 1) which have a similar substitution pattern at the 6-position.

The 2′-Cl phenyl group in **11a**, 4′-Cl benzyl group in **12a**, and 3′,4′-diCl benzyl in group in **15a** would afford information on activity obtained on having an electron withdrawing group (or groups) at the respective positions. The 3′,4′,5′-triOMe benzyl group in **19a** would afford information on activity obtained on having electron donating groups at these positions.

The 1-naphthyl moiety in **16a**, 2-naphthyl in **17a**, and 4′-phenyl benzyl group in **18a** were included to obtain information about bulk tolerance in this position in the RTK active site.

2. Chemistry

The synthesis of compounds **9a**–**19a** is shown in Scheme 1. Compound **26** was obtained by cyclocondensation of chloroacetaldehyde **25** with **24** at reflux for 4 h as previously reported.[27] Chlorination of **26** with phosphorus oxychloride, in the presence of *N*,*N*′-dimethylaniline as a catalyst afforded **27**. Nucleophilic displacement of the 4-chloro group in **27** with 3-bromoaniline **28** furnished the common intermediate **29**. The target compounds **9a**–**19a** were obtained in yields ranging from 5% to 47% by a sodium hydride induced regiospecific alkylation of **29** at the 7-position with the corresponding substituted arylmethyl halides **30a–k**. The purification of the target compounds was tedious since the by-products had R_f values (TLC) close to the desired compounds **9a–19a**. This necessitated the exploration of alternate synthetic procedures, particularly for large scale synthesis of the compounds for in vivo evaluation.

A gram scale synthesis of **11a** was accomplished by an improved method[28] as shown in Scheme 2. A sodium hydride induced alkylation of the N7-position of **27** furnished **31**. This was followed by a nucleophilic displacement of the 4-chloro group in **31** with **28** to afford **11a**. This modified protocol provided a remarkable improvement in the overall reaction yield of **27** to **11a** from a mere 5% (Scheme 1) to 39% (Scheme 2).

3. Biological evaluation and discussion

The RTK inhibitory activities of compounds **9a**–**19a** (Table 1) were evaluated using a phosphotyrosine ELISA in human tumor cells known to express high levels of EGFR, VEGFR-1, VEGFR-2, and PDGFR*β*.[29,30] Compounds known to inhibit a specific RTK were used as a positive control for these assays. Whole cell assays were used for measuring RTK inhibition as these assays afford more meaningful results for translation to in vivo studies.[25,31–34] To study the effect of compounds on cell proliferation, A431 cancer cells known to over express EGFR were used. EGFR has been shown to be a factor in the overall survival of A431 cells.[26] Cell-proliferation was measured using CYQUANT®, a DNA intercalating dye shown to provide a linear approximation of cell number.[35] In this assay, purified angiogenic growth factors are positioned locally on a vascularized membrane of a developing chicken embryo along with possible inhibitors. Digitized images of the vasculature are taken 48 h after growth factor administration and the number of vessels per unit area is quantified to measure vascular density.

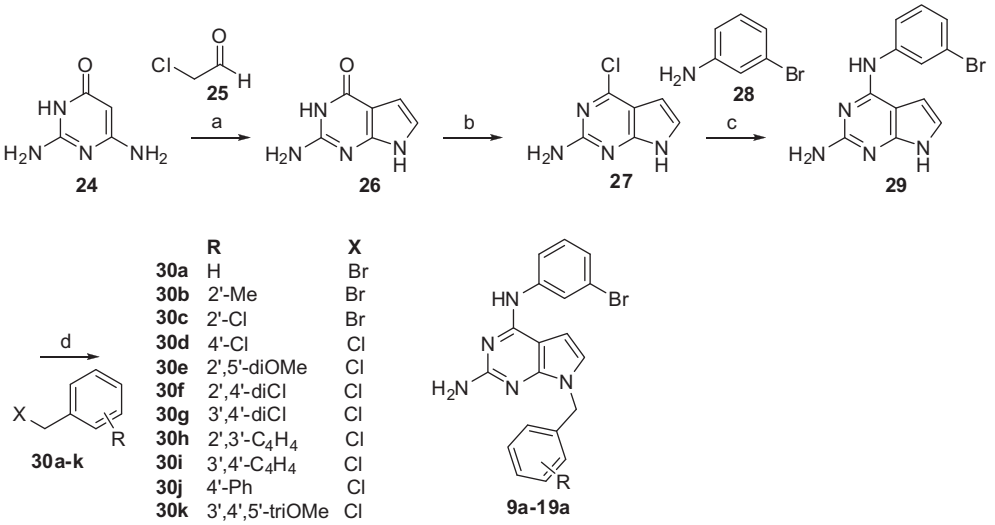

Scheme 1. Reagents and conditions: (a) sodium acetate, water, reflux, 4 h; (b) phosphorus oxychloride, *N*,*N*′-dimethylaniline, reflux, 4 h; (c) isopropanol, three drops concd HCl, reflux, 4 h; (d) sodium hydride, dimethylformamide, 0 °C–1 h, rt–10 min-4 h.

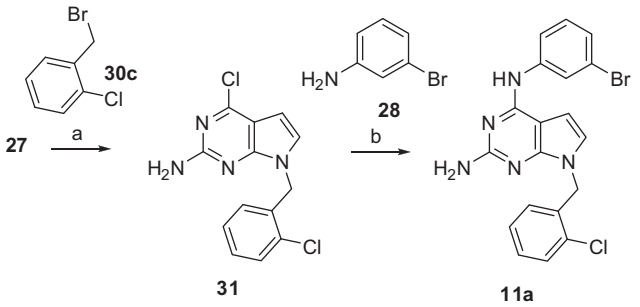

Scheme 2. Reagents and conditions: (a) sodium hydride, dimethylformamide, 0 °C–30 min, rt–2 h; (b) isopropanol, three drops concd HCl, reflux, 4 h.

The IC_{50} values of RTK inhibition vary under different assay conditions. Hence, we used a standard (control) compound in each of the evaluations. For EGFR, the standard was **20** (Fig. 1); for VEGFR-1 the standard was **21**; for VEGFR-2 the standard was **7**; for PDGFRβ the standard was **22**; for the cytotoxicity study against the growth of A431 cells in culture the standards were **20**, **7** and **23**.

Since the inhibitory activities are determined in cells, a definite structure–activity relationship cannot be determined for **9a**–**19a** and RTK inhibition. Compounds **11a** with a 2′-Cl benzyl substitution and **19a** with a 3′,4′,5′-triOMe benzyl substitution inhibited PDGFRβ at single digit micromolar concentrations. Compounds **11a** and **19a** inhibited PDGFRβ fourfold and threefold better respectively than the standard **22**. The 2′,4′-diCl benzyl substituted **14a**, inhibited PDGFRβ at an IC_{50} 5.5-fold lower than **22**. Compounds **16a** (1-naphthyl substituted) and **18a** (4-phenyl benzyl substituted) had similar potencies and were 20-fold less active than **22**. The 2-naphthyl substituted **17a** was 34-fold less potent than **22**. Hence bulky 7-substituents were not tolerated (**16a**–**18a**). An electron withdrawing group at the 2′-position (2′-Cl benzyl in **11a**) is favorable for activity, but an electron donating group in this position (2′-Me benzyl in **10a**), or an unsubstituted phenyl (**9a**) is not favored. Moving the 2′-chloro group to the 4′-position (compare **11a** to **12a**), or disubstitution with chloro groups (**14a**, **15a**) is detrimental to activity. The most active compound in the parent series in this assay is the 2′,5′-diOMe benzyl substituted **13**. The most active compound in the N7 substituted series, the 2′-Cl benzyl substituted **11a** is >33-fold more active than its parent regioisomer **11**.

In the VEGFR-2 assay, compounds **9a** with an unsubstituted phenyl was twofold less potent than the standard **23**. The 2-naphthyl substituted **17a** was also twofold less active than **23**, while the 1-naphthyl substituted **16a** was 1.4-fold less active than **23** and was the most active compound in this series, in the VEGFR-2 assay. The electron withdrawing 2′-Cl benzyl substituted **11a** was the next most active compound and was 1.6-fold less active than **23**; however the electron donating 2′-Me benzyl substituted **10a** was 11-fold less potent than **23**. Comparison of **11a** and **10a**, suggests that an electron withdrawing substituent at the 2′-position is beneficial for activity relative to an electron donating group. The 4′-Cl benzyl substituted **12a** was sixfold less active than **23**, while the 2′,4′-diCl benzyl substituted **14a** was inactive. The 3′,4′-diCl benzyl substituted **15a** was also sixfold less active than **23**. The 4-phenyl benzyl substituted **18a** was only twofold less active than **23** indicating that bulk is tolerated in this position. The 3′,4′,5′-triOMe benzyl substituted **19a** was also twofold less active than **23**. The 2′,5′-diOMe benzyl substituted **13a** was inactive even at 200 μM. The most active compound in the parent series, the 2′-Me benzyl substituted **10**, is 450-fold more active relative to its regioisomer **10a**. The most active compound in the N7 substituted series, the 1-naphthyl substituted **16a** is threefold less active than its parent regioisomer **16**.

In the VEGFR-1 assay, compound **9a**, with an unsubstituted benzyl group was 5.6-fold less active than the standard **21**. Compound **10a** has a methyl group in the 2′ position of the benzyl substituent (compared to **9a**). This compound is sevenfold less active than standard **21**. Compound **11a** bears a 2′-chloro benzyl substituent and is also sevenfold less active than **21**. The 2′-substituted compounds **10a** and **11a** were less active than the unsubstituted **9a**. Compound **16a** with a (naphthalene-1-yl)methyl substitution, and, bulk at the 2′ position, is 8.4-fold less active than **21**. Conversely the (naphthalene-2-yl)methyl substitution in compound **17a** is beneficial for activity, with this compound being only 2.8-fold less active than **21** and the most potent compound in this series against VEGFR-1. Compound **12a** with a 4′-Cl benzyl is 4.5-fold less active than **21**; while **11a** with a 2′-Cl benzyl is sevenfold less active than **19**. Excessive bulk in the 4′-position is not tolerated as exemplified by the (biphenyl-4-yl)methyl substituted **18a** which is inactive at a concentration of 200 μM. Dichloro benzyl substituted compounds **14a** and **15a** were eight- and sevenfold less active than **21** respectively. The 2′,5′-dimethoxy benzyl substituted compound

is inactive at 200 μM. The 3′,4′,5′-triOMe benzyl substituted compound **19a**, which lacks the 2′-substitution is about 8.8-fold less active than **21**. Compared to the parent 6-benzyl substituted series, **9a**–**19a** showed a decrease in VEGFR-1 inhibition.

In the EGFR assay, the 2′,5′-dimethoxy benzyl substituted compound **13a** exhibited 2-digit micromolar inhibition. Though this compound was the most potent compound of the series in this assay, its activity was 346-fold lower than the standard **20**. Compounds **10a** with a 2′-Me benzyl and **12a** with a 4′-Cl benzyl substitution were about 500-fold less potent than **20**. Compound **9a** with an unsubstituted phenyl group was about 800-fold less active than **20**. EGFR inhibition was abolished on variations with a bulky substitution (1-naphthyl methyl in **16a**, 2-naphthyl methyl in **17a**, and 4-phenyl benzyl in **18a**). In addition, alternative di-substitution (2′,4′-diCl benzyl in **14a**, 3′,4′-diCl benzyl in **15a**) and tri-substitution (3′,4′,5′-triOMe benzyl in **19a**) also lead to inactivity in the EGFR assay. Relative to the parent 6-benzyl substituted series (**9**–**19**), **9a**–**19a** showed a decrease in activity in the EGFR assay.

The most potent compound, in the A431 cytotoxicity assay, the 4-phenyl benzyl substituted **18a** was equipotent to standard **20**, 1.4-fold better than **7** and 1.7-fold less active than **23**. The 2′-Me benzyl substituted **10a**, 4′-Cl benzyl substituted **12a**, and 2′,4′-diCl benzyl substituted **14a** were equipotent to the standard **20**, and 1.2-fold more potent than **7**. Every compound had an improved A431 cytotoxicity value relative to their corresponding EGFR kinase IC_{50}'s. This is presumably due to the varied transport and/or pharmacokinetic differences of analogs between the two cell systems.

Taken together, transposing the 6-benzyl substituent in the parent compounds to the 7-position produced significant differences in the inhibition of the various RTKs. Although the EGFR inhibition present in the parent series was lost in **9a**–**19a**, some of these compounds (**11a**, **19a**) were much more potent PDGFRβ inhibitors. The variation in activity of analogs **9a**–**19a** may either be due to the stringent requirements for binding in individual RTKs and/or due to differences in cell permeability of these compounds.

From this study, compounds **11a** and **19a** were identified as inhibitors of multiple RTKs. The discovery of these compounds is significant because they are potent inhibitors of VEGFR-2. In addition, **11a** and **19a** inhibit PDGFRβ at concentrations better than the standard agents. As stated above VEGFR-2 and PDGFRβ are the two principal mediators of angiogenesis. Compared to the most potent multikinase inhibitor **11a**, the most potent multikinase inhibitor in the parent series—compound **13**—had a 2′,5′-diOMe benzyl group at N6 and exhibited inhibition against PDGFRβ at values 1.5-fold less than the standard **22** and in addition, demonstrated VEGFR-2 inhibition 17-fold better than the standard **23** (Table 1).

4. Molecular modeling studies

Molecular modeling studies were carried out using Flexx 3.1.2[36] and MOE 2008.10[37] in VEGFR2 (pdb code 1YWN)[38] and a homology model of PDGFRβ.[39] Figures 3–5 depict the docked poses of **11** and its regioisomer **11a** as a representative study in VEGFR2 and the homology model of PDGFRβ. Figure 3 shows the superimposition of the best scored docked poses of **11** and **11a** in the ATP binding site of VEGFR-2. The binding site of ATP competitive inhibitors in RTKs consists of a Hinge region, two hydrophobic binding sites (Hydrophobic region I and II) and a Sugar binding pocket (Fig. 3).[25,40–42] Compounds **11** and **11a** can be seen to adopt different docked conformations in the active site. The pyrrolo[2,3-*d*]pyrimidine ring of **11a** occupies the adenine binding portion of the ATP binding site. The 2-NH_2 moiety is involved in a hydrogen bond with Glu915 in the Hinge region while the N3 and 4-anilino NH are involved in hydrogen bonds with the backbone of Cys917 in the Hinge region. Additional hydrophobic interactions of the pyrrolo[2,3-*d*]pyrimidine ring with Leu1033 (not labeled) can stabilize the docked pose. In this pose, the N7 benzylic substitution extends towards Hydrophobic region I and is involved in interactions with Val846, Ala864, Val897 and Val914. The N7 benzylic substitution also interacts with the side chain carbon atoms of Glu883 and Cys1043. The N^4-(3-bromophenyl) is extended towards Hydrophobic region II and interacts with the side chains of Phe916, Leu838 (not shown) and Leu1033 (not shown).

In contrast, the pyrrolo[2,3-*d*]pyrimidine scaffold of **11** docks in a flipped conformation compared to **11a** described above that enables the formation of three hydrogen bonds with the hinge region (Fig. 3). The 2-NH_2, N1 and pyrrole NH of **11** form hydrogen bonds with the backbone of Glu915 and Cys917. Additionally, the pyrrolo[2,3-*d*]pyrimidine scaffold forms hydrophobic interactions with Leu838 (not shown), Val846, Ala864, Val897 and Leu1033 (not shown). This mode places the N^4-(3-bromophenyl) moiety in Hydrophobic region I where it forms hydrophobic interactions with Val846, Ala864, Leu887, Val897, Val912 and Val914. Additional hydrophobic interactions with the side chain carbon atoms of Lys866 and Glu883 stabilize this docked pose. The 6-benzylic substitution extends towards Hydrophobic region II and forms interactions with Leu838 (not shown), side chain atoms of Phe916, Cys917, Lys918 and Gly920 (not shown). Thus, molecular modeling and docking studies suggests that the 7-benzylic substitution forces **11a** to adopt a binding mode different from that docked for the 6-benzylic compound **11** in VEGFR2.

There is no reported crystal structure of PDGFRβ bound to a ligand. Hence a homology model of PDGFRβ was built using the structure of c-KIT kinase complex (pdb code 1PKG) as a template.[30] Docking studies were performed with **11** and **11a** as described above for VEGFR-2. Compound **11a** binds to the ATP binding site of PDGFRβ with the pyrrolo[2,3-*d*]pyrimidine portion occupying the adenine binding site (Fig. 4). Critical hydrogen bonds with the Hinge region are maintained in this binding mode: the aniline NH hydrogen bonds with the backbone of Cys684 while the N3 and 2-NH_2 moieties form hydrogen bonds with Glu682. This binding mode places the N^4-(3-bromophenyl) moiety in Hydrophobic region I and forms hydrophobic interactions with Val614, Ala632 (not shown), Val665 and Leu833 (not shown) and with the side chain carbon atoms of Lys634 andThr681. The N7-benzyl substituent lies in the Sugar binding pocket where it can interact with Leu606 (not shown), Val614, Val615 (not shown) and Ala848. A similar binding mode was seen with the best scored pose of **11** in PDGFRβ. The 6-benzylic substituent of **11** accesses the same region accessed by the 7-benzylic substituent of **11a** however in a different conformation as shown in Figure 4. It was interesting to note that alternate binding modes of **11a** that scored 1-2 kcal/mol higher than the best docked pose indicate different bound conformations of the 7-benzylic substituent (Fig. 5). In the alternate binding mode, the 7-benzylic substituent accesses Hydrophobic region II instead of the sugar binding pocket as is seen in the bound conformation in Fig. 5 where it interacts with Phe916 and Leu938 (not shown). Compound **11**, which has a 6-benzylic substituent cannot access Hydrophobic region II in the poses seen in Figures 3 and 4. Similar poses were observed from the docking studies on other compounds. These binding modes suggested that the presence of multiple docked poses could translate into differences in the activity and selectivity of these compounds against different kinases as compared to the parent series.

On the basis of its in vitro activity, compound **11a** was selected for in vivo evaluation in a mouse model to determine its effect on tumor growth, metastasis, and angiogenesis.

To examine whether compound **11a** was effective in vivo in reducing tumor volume and metastasis, a syngeneic mouse tumor model was used. Athymic mice implanted with COLO-205 meta-

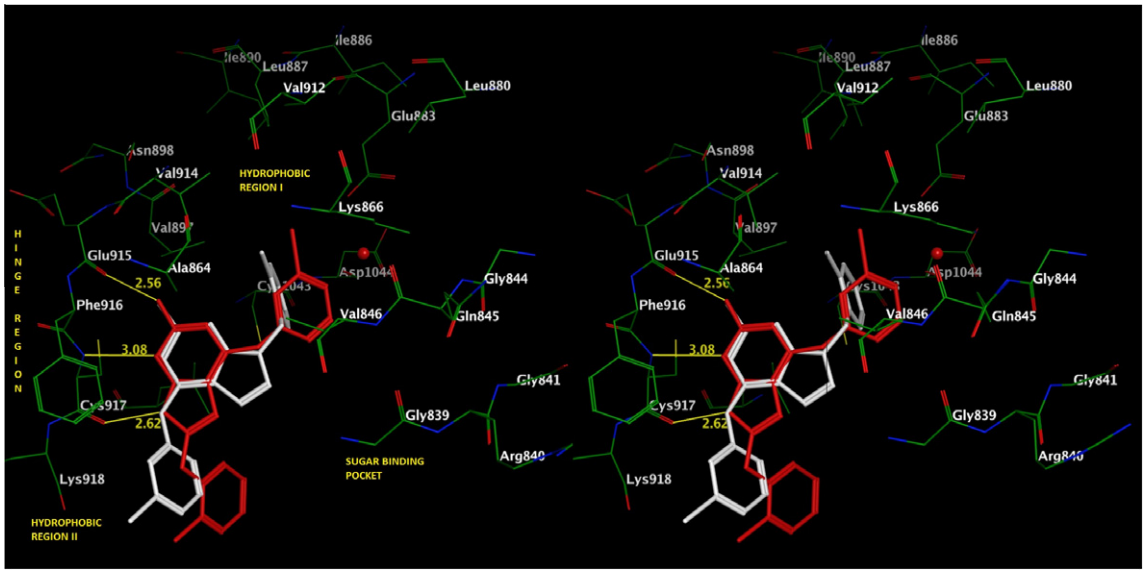

Figure 3. Stereo view. Superimposition of docked poses of **11** (red) and **11a** (white) in the ATP binding site of VEGFR2 (PDB: 1YWN).

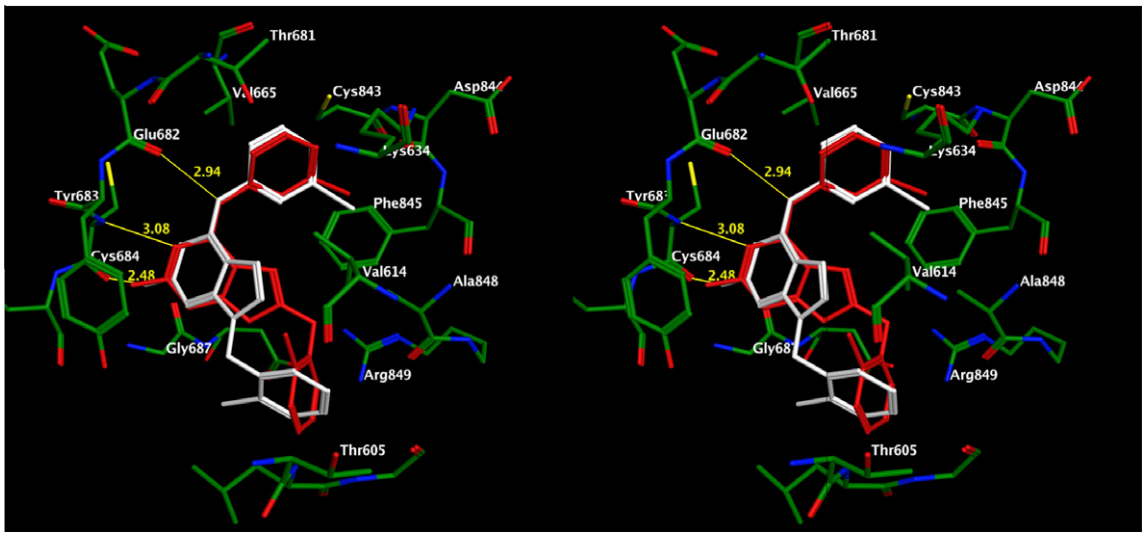

Figure 4. Stereo view of the docked pose of **11** (red) and **11a** (white) in the putative binding site of PDGFRβ. The putative binding site of PDGFRβ was generated by homology modeling.[30]

static colon cancer cells, shown to overexpress PDGFRβ were used.[43] In a six week toxicity determination study, it was found that 35 mg/kg of **11a** and 10 mg/kg (MTD) **8**[44] caused no overt toxicity in mice (data not shown). At day 10 after implantation, the multitargeted inhibitor **8** at the MTD of 10 mg/kg three times weekly and **11a** at 35 mg/kg three times weekly were administered to mice (Fig. 6A). Tumor growth was measured using calipers. It was found that **8** and **11a** resulted in significant decreases in primary tumor growth rate (Fig. 6B) compared to the control. At the end of the experiment, tumors were taken and stained for blood vessels as described in the methods section. It was found that both **8** and **11a** resulted in a significant decrease in primary tumor vascularity as compared to control animals (Fig. 6C). Finally, livers were stained for the presence of metastases and it was found that **11a**, but not **8**, resulted in significantly reduced numbers of COLO-205 metastases to the liver (Fig. 6D). Thus **11a** demonstrated significant tumor inhibitory activity, antiangiogenic activity and antimetastatic activity in a COLO-205 mouse tumor xenograft model and is being considered for further preclinical development.

In summary, eleven novel N^4-(3-bromophenyl)-7-(substitutedbenzyl) pyrrolo[2,3-*d*]pyrimidines **9a**–**19a** were designed and synthesized as RTK inhibitors. The biological evaluation showed that several analogs afforded potent inhibition against PDGFRβ, VEGFR-2 and the A431 cytotoxicity assay. Of the analogs evaluated, **11a** and **19a** were better than or comparable to the standard compounds used in these assays against two principal RTKs responsible for angiogenesis in tumors—PDGFRβ and VEGFR-2. Compound **11a** was evaluated in a COLO-205 xenograft mouse model, where it exhibited tumor growth inhibition, antimetastatic and antiangiogenic effects better than or comparable to standard **8**. Using the analogs described in this study as leads, structure based design and synthesis of novel multi-RTK inhibitors are currently in progress. In addition, selected compounds from this study are being evaluated in preclinical studies and in other tumor xenograft as-

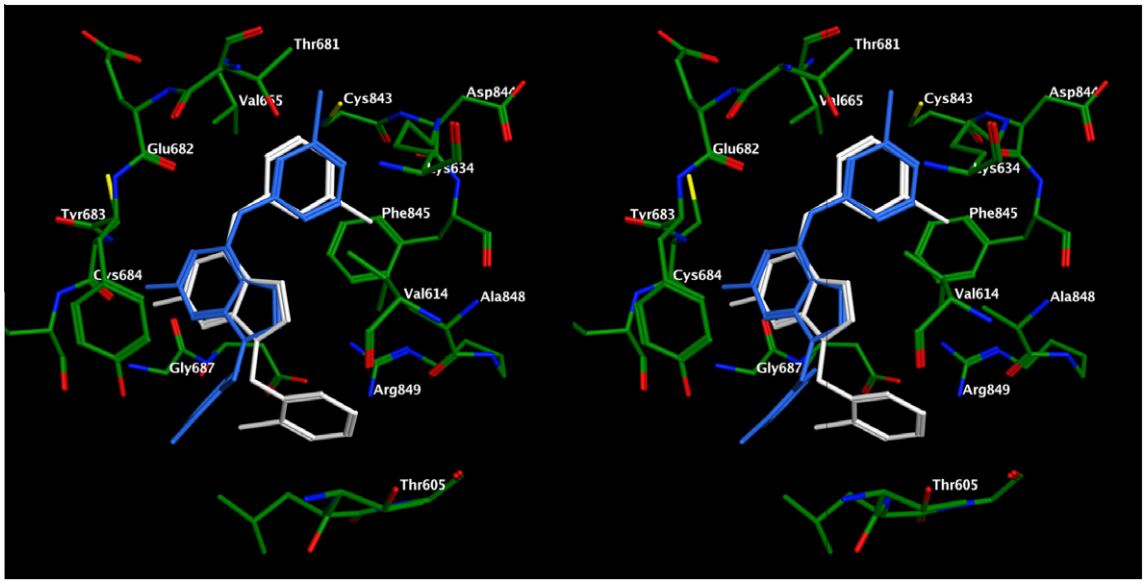

Figure 5. Stereo view. Superimposition of the best scored pose (white) and alternate docked pose (blue) of **11a** in the putative binding site of PDGFRβ. The putative binding site of PDGFRβ was generated by homology modeling.[39]

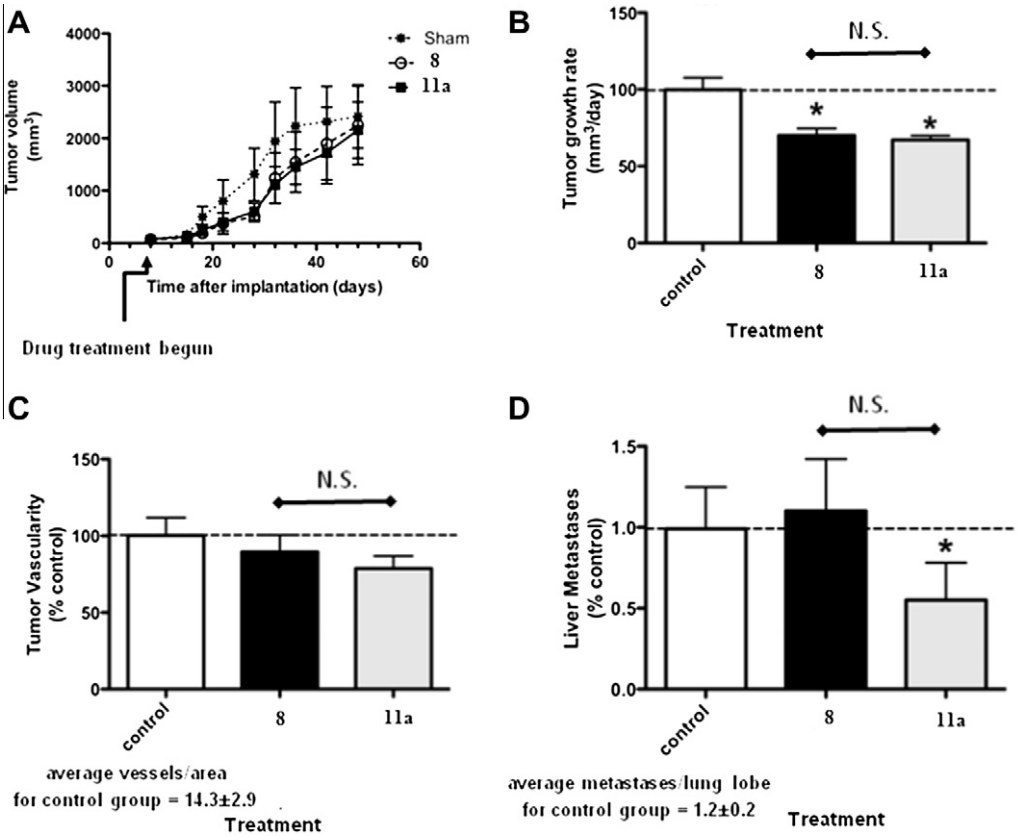

Figure 6. Tumor growth (A), primary tumor growth rate (B), primary tumor vascularity (C), and liver metastasis of COLO-205 tumor xenografts after various treatments (D). COLO-205 cells were implanted into male athymic mice as in the research design and methods section. Compounds were administered at the listed doses three times weekly and tumor growth measured using calipers. At the experiment end, tumors were stained for vascularity and livers stained for metastases as in research design and methods section. Data represent the average ± SD of 6–9 animals. $^{*}P > 0.05$, $^{**}P < 0.01$, $^{***}P < 0.001$ by one way ANOVA and Repeated Measures post test. The average tumor growth rate for control treated animals (B) is 100.2 mm^3/day, average number of tumor vessels in control-treated animals are 14.3/field (C) and average metastases in control treated animals are 1.2/lobe.

says. One of the observed differences on transposing the 6-benzyl substituent in the parent compounds to the 7-position was that—although the EGFR inhibition present in the parent series was lost in **9a**–**19a**, some of these compounds (**11a**, **19a**) were much more potent PDGFRβ inhibitors. Molecular modeling studies indicate that access of Hydrophobic region II by the 7-benzyl substituent

in this series could explain, in part, the observed differences in activities as compared to the 6-substituted lead series of compounds.

5. Experimental section

Analytical samples were dried in vacuo (0.2 mm Hg) in a CHEM-DRY drying apparatus over P_2O_5 at 80 °C. Melting points were determined on a MEL-TEMP II melting point apparatus with FLUKE 51 K/J electronic thermometer and are uncorrected. Nuclear magnetic resonance spectra for proton (^{1}H NMR) were recorded on a Bruker WH-300 (300 MHz) or a Bruker 400 MHz/52 MM (400 MHz) spectrometer. The chemical shift values are expressed in ppm (parts per million) relative to tetramethylsilane as an internal standard: s, singlet; d, doublet; t, triplet; q, quartet; m, multiplet; br, broad singlet. Thin-layer chromatography (TLC) was performed on Whatman Sil G/UV254 silica gel plates with a fluorescent indicator, and the spots were visualized under 254 and 366 nm illumination. Proportions of solvents used for TLC are by volume. Column chromatography was performed on a 230–400 mesh silica gel (Fisher, Somerville, NJ) column. Elemental analyses were performed by Atlantic Microlab, Inc., Norcross, GA. Element compositions are within (0.4% of the calculated values and indicate >95% purity. Fractional moles of water or organic solvents frequently found in some analytical samples could not be prevented in spite of 24–48 h of drying in vacuo and were confirmed where possible by their presence in the ^{1}H NMR spectra. All solvents and chemicals were purchased from Aldrich Chemical Co. or Fisher Scientific and were used as received. High resolution mass spectra (HRMS) were obtained for compounds **13a** and **18a** and TLC of these compounds produced a single spot in three different solvent systems.

5.1. 4-Chloro-7*H*-pyrrolo[2,3-*d*]pyrimidin-2-amine (27)

To a round-bottomed flask were added **26** (3 g, 19.9 mmol) of and three drops of *N*,*N*′-dimethyl aniline. The mixture was suspended on phosphorus oxychloride (250 mL). The reaction was continued at reflux for 4 h. After cooling to room temperature, the solvent was evaporated under reduced pressure and the residue was treated with ice water (20 mL) in an ice bath. The pH of the suspension was adjusted to 7 with concentrated ammonium hydroxide solution. The precipitate was filtered, air-dried and then dissolved in methanol. Silica gel (6 g) was added to the solution which was then evaporated to dryness to form a plug. The silica gel plug obtained was loaded onto a silica gel column and eluted with 2% methanol in chloroform. Fractions corresponding to the product (TLC) were pooled and evaporated to dryness under reduced pressure to afford **27** (10%) as a sparkling white solid: mp 215–216 °C; TLC R_f 0.56 ($CHCl_3$/CH_3OH, 5:1 with two drops of concentrated NH_4OH); ^{1}H NMR (DMSO-d_6): δ 6.24 (s, 1H, C5–CH), 6.49 (br s, 2H, NH_2, exch), 7.08 (s, 1H, C6–CH), 11.46 (s, 1H, NH, exch). Anal. ($C_6H_5ClN_4 \cdot 0.25H_2O$) C, H, N, Cl.

5.2. N^4-(3-Bromophenyl)-7*H*-pyrrolo[2,3-*d*]pyrimidine-2,4-diamine (29)

To a round bottomed flask were added **27** (111 mg, 0.65 mmol)and 3-bromoaniline **28** (226 mg, 1.31 mmol) in isopropanol (10 mL). Following this three drops of concd HCl were added. The reaction was continued at reflux for 4 h at the end of which the solvent was evaporated under reduced pressure. The residue was dissolved in methanol (10 mL), and silica gel (250 mg) was added to the solution which was then evaporated to dryness to form a plug. The silica gel plug obtained was loaded onto a silica gel column and eluted with 2% methanol in chloroform. Fractions corresponding to the product (TLC) were pooled and evaporated to dryness under reduced pressure to afford **29** (70%) as a green solid: mp 210–212.5 °C; TLC R_f 0.56 ($CHCl_3$/CH_3OH, 5:1 with two drops of concentrated NH_4OH); ^{1}H NMR (DMSO-d_6): δ 5.81 (br s, 2H, NH_2, exch), 6.55 (s, 1H, C5–CH), 6.79 (s, 1H, C6–CH), 7.11 (s, 1H, Ar–H), 7.22 (d, J = 12 Hz, 1H, Ar–H), 8.05 (d, J = 12 Hz, 1H, Ar–H), 8.14 (s, 1H, Ar–H), 9.04 (s, 1H, NH, exch), 10.91 (s, 1H, NH, exch). Anal. ($C_{12}H_{10}BrN_5 \cdot 0.1H_2O$) C, H, N, Br.

5.3. General procedure for the synthesis of compounds 9a–19a

To a round bottomed flask was added **29** and dissolved in 5 ml of DMF. The solution was cooled to 0 °C and sodium hydride was added. After stirring at 0 °C for 1 hour, the appropriate (halomethyl)arene was added. The reaction was continued at rt till the appearance of a new spot (TLC) after which the reaction was quenched with water. The water phase was extracted with chloroform. The organic phase was dried over sodium sulfate and evaporated under reduced pressure. The residue was dissolved in methylene chloride, 250 mg silica gel was added to the solution which was then evaporated to dryness to form a plug. The silica gel plug obtained was loaded onto a silica gel column and eluted with 1% methanol in chloroform. Fractions corresponding to the product (TLC) were pooled and evaporated to dryness under reduced pressure to afford the product.

5.4. 7-Benzyl-N^4-(3-bromophenyl)-7*H*-pyrrolo[2,3-*d*]pyrimidine-2,4-diamine (9a)

Reaction of **29** (210 mg, 0.69 mmol), **30a** (236 mg, 1.38 mmol) and sodium hydride (16 mg, 0.65 mmol), using the general procedure described above, gave **11a**: yield 36%, mp >200 °C; TLC R_f 0.87 ($CHCl_3$/CH_3OH, 10:1 with two drops concentrated NH_4OH); ^{1}H NMR (DMSO-d_6): δ 5.30 (s, 2H, CH_2), 6.03 (br s, 2H, NH_2, exch), 6.60 (d, J = 9 Hz, 1H, Ar–H), 6.71 (s, 1H, C5–CH), 6.91 (s, 1H, C6–CH), 7.12–7.15 (s, 1H, Ar–H), 7.22–7.31 (m, 4H, Ar–H), 7.49–7.51 (m, 2H, Ar–H), 8.07–8.13 (m, 2H, Ar–H), 9.17 (s, 1H, NH, exch). Anal. ($C_{19}H_{16}N_5Br \cdot 5CHCl_3$) C, H, N, Br.

5.5. N^4-(3-Bromophenyl)-7-(2-methylbenzyl)-7*H*-pyrrolo[2,3-*d*]pyrimidine-2,4-diamine (10a)

Reaction of **29** (500 mg, 1.64 mmol), **30b** (607 mg, 3.28 mmol) and sodium hydride (39 mg, 1.64 mmol), using the general procedure described above, gave **10a**: yield 34%, mp 177 °C; TLC R_f 0.85 ($CHCl_3$/CH_3OH, 5:1 with two drops concentrated NH_4OH); ^{1}H NMR (DMSO-d_6): δ 2.30 (s, 3H, CH_3), 5.19 (s, 2H, CH_2), 5.97 (br s, 2H, NH_2, exch), 6.61 (m, 1H, Ar–H), 6.65 (s, 1H, C5–CH), 6.77 (s, 1H, C6–CH), 7.05–7.27 (m, 5H, Ar–H), 7.95–8.13 (m, 2H, Ar–H), 9.12 (s, 1H, NH, exch). Anal. ($C_{20}H_{18}N_5Br$) C, H, N, Br.

5.6. N^4-(3-Bromophenyl)-7-(2-chlorobenzyl)-7*H*-pyrrolo[2,3-*d*]pyrimidine-2,4-diamine (11a)

Method A: Reaction of **29** (200 mg, 0.65 mmol), **30c** (270 mg, 1.31 mmol) and sodium hydride (15 mg, 0.62 mmol), using the general procedure described above, gave **11a**: yield 7%.

Method B: To a round bottomed flask were added **31** (320 mg, 1.1 mmol)and 3-bromoaniline **28** (1.42 g, 8.25 mmol) in isopropanol (10 mL), followed by the addition of three drops of concd HCl. The reaction was continued at reflux for 4 h at the end of which the solvent was evaporated under reduced pressure. The residue was dissolved in methanol (10 mL), and silica gel gel (3 g) was added to the solution which was then evaporated to dryness to form a

plug. The silica gel plug obtained was loaded onto a silica gel column and eluted with plain chloroform. Fractions corresponding to the product (TLC) were pooled and evaporated to dryness under reduced pressure to afford **11a** (81%) as a white solid: mp 182.8 °C; TLC R_f 0.87 ($CHCl_3/CH_3OH$, 5:1 with two drops concentrated NH_4OH); ^1H NMR (DMSO-d_6): δ 5.28 (s, 2H, CH_2), 6.02 (br s, 2H, NH_2, exch), 6.59 (d, J = 6 Hz, 1H, Ar–H), 6.68 (s, 1H, C5–CH), 6.89 (s, 1H, C6–CH), 7.12 (d, J = 6 Hz, 1H, Ar–H), 7.21–7.29 (m, 3H, Ar–H), 7.49 (d, J = 9 Hz, 1H, Ar–H), 8.05–8.11 (m, 2H, Ar–H), 9.17 (s, 1H, NH, exch). Anal. ($C_{19}H_{15}N_5BrCl$) C, H, N, Br, Cl.

5.7. N^4-(3-Bromophenyl)-7-(4-chlorobenzyl)-7*H*-pyrrolo[2,3-*d*] pyrimidine-2,4-diamine (12a)

Reaction of **29** (200 mg, 0.65 mmol), **30d** (211 mg, 1.31 mmol) and sodium hydride (15 mg, 0.62 mmol), using the general procedure described above, gave **12a**: yield 47%, mp 127–128 °C; TLC R_f 0.88 ($CHCl_3/CH_3OH$, 10:1 with two drops concentrated NH_4OH); ^1H NMR (DMSO-d_6): δ 5.19 (s, 2H, CH_2), 6.04 (br s, 2H, NH_2, exch), 6.63 (d, J = 3 Hz, 1H, C5–CH), 6.89 (d, J = 3 Hz, 1H, C6–CH), 7.14–8.09 (m, 8H, Ar–H), 9.14 (s, 1H, NH, exch). Anal. ($C_{19}H_{15}N_5BrCl$) C, H, N, Br, Cl.

5.8. N^4-(3-Bromophenyl)-7-(2,5-dimethoxybenzyl)-7*H*-pyrrolo [2,3-*d*]pyrimidine-2,4-diamine (13a)

Reaction of **29** (300 mg, 0.98 mmol), **30e** (368 mg, 1.97 mmol) and sodium hydride (22 mg, 0.93 mmol), using the general procedure described above, gave **13a**: yield 10%, mp 150.9 °C; TLC R_f 0.71 ($CHCl_3/CH_3OH$, 10:1 with two drops concentrated NH_4OH); ^1H NMR (DMSO-d_6): δ 3.56 (s, 3H, OCH_3), 3.79 (s, 3H, OCH_3), 5.11 (s, 2H, CH_2), 6.00 (br s, 2H, NH_2, exch), 6.11 (s, 1H, Ar–H), 6.64 (d, J = 3 Hz, 1H, C5-CH), 6.77–6.79 (m, 1H, Ar–H), 6.85 (d, J = 3 Hz, 1H, C6-CH), 6.92–8.11 (m, 5H, Ar–H), 9.13 (s, 1H, NH, exch). HRMS calcd for $C_{21}H_{20}N_5O_2Br$ 453.0800, found 453.0788.

5.9. N^4-(3-Bromophenyl)-7-(2,4-dichlorobenzyl)-7*H*-pyrrolo [2,3-*d*]pyrimidine-2,4-diamine (14a)

Reaction of **29** (100 mg, 0.32 mmol), **30f** (125 mg, 0.64 mmol) and sodium hydride (7 mg, 0.32 mmol), using the general procedure described above, gave **14a**: yield 24%, mp 191.4 °C; TLC R_f 0.86 ($CHCl_3/CH_3OH$, 5:1 with two drops concentrated NH_4OH); ^1H NMR (DMSO-d_6) δ 5.26 (s, 2H, CH_2), 6.05 (br s, 2H, NH_2, exch), 6.58 (d, J = 6 Hz, 1H, Ar–H), 6.69 (s, 1H, C5–CH), 6.89 (s, 1H, C6–CH), 7.13–7.35 (m, 3H, Ar–H), 7.67 (s, 1H, Ar–H), 8.07–8.11 (m, 2H, Ar–H), 9.18 (s, 1H, NH, exch). Anal. ($C_{19}H_{14}N_5BrCl_2$) C, H, N, Br, Cl.

5.10. N^4-(3-Bromophenyl)-7-(3,4-dichlorobenzyl)-7*H*-pyrrolo [2,3-*d*]pyrimidine-2,4-diamine (15a)

Reaction of **29** (200 mg, 0.65 mmol), **30g** (256 mg, 1.31 mmol) and sodium hydride (15 mg, 0.62 mmol), using the general procedure described above, gave **15a**: yield 16%, mp 136.3 °C; TLC R_f 0.78 ($CHCl_3/CH_3OH$, 10:1 with two drops concentrated NH_4OH); ^1H NMR (DMSO-d_6) δ 5.20 (s, 2H, CH_2), 6.02 (br s, 2H, NH_2, exch), 6.64 (d, J = 3 Hz, 1H, C5–CH), 6.92 (d, J = 3 Hz, 1H, C6–CH), 7.09–8.10 (m, 7H, Ar–H), 9.13 (s, 1H, NH, exch). Anal. ($C_{19}H_{14}BrCl_2N_5{\cdot}0.25CHCl_3$) C, H, N, Br, Cl.

5.11. N^4-(3-Bromophenyl)-7-(1-naphthylmethyl)-7*H*-pyrrolo [2,3-*d*]pyrimidine-2,4-diamine (16a)

Reaction of **29** (500 mg, 1.64 mmol), **30h** (579 mg, 3.28 mmol) and sodium hydride (39 mg, 1.64 mmol), using the general procedure described above, gave **16a**: yield 18%, mp 237.5 °C; TLC R_f 0.92 ($CHCl_3/CH_3OH$, 5:1 with two drops concentrated NH_4OH); ^1H NMR (DMSO-d_6): δ 5.67 (s, 2H, CH_2), 6.01 (br s, 2H, NH_2, exch), 6.64 (d, J = 3 Hz, 1H, C5–CH), 6.82 (d, J = 3 Hz, 1H, C6–CH), 6.93–8.21 (m, 11H, Ar–H), 9.12 (s, 1H, NH, exch). Anal. ($C_{23}H_{18}N_5Br$) C, H, N, Br.

5.12. N^4-(3-Bromophenyl)-7-(2-naphthylmethyl)-7*H*-pyrrolo [2,3-*d*]pyrimidine-2,4-diamine (17a)

Reaction of **29** (200 mg, 0.65 mmol), **30i** (290 mg, 1.31 mmol) and sodium hydride (15 mg, 0.62 mmol), using the general procedure described above, gave **17a**: yield 19%, mp 130.2 °C; TLC R_f 0.73 ($CHCl_3/CH_3OH$, 10:1 with two drops concentrated NH_4OH); ^1H NMR (DMSO-d_6): δ 5.37 (s, 2H, CH_2), 5.98 (br s, 2H, NH_2, exch), 6.65 (d, J = 3 Hz, 1H, C5–CH), 6.92 (d, J = 3 Hz, 1H, C6–CH), 7.12–8.12 (m, 11H, Ar–H), 9.11 (s, 1H, NH, exch). HRMS calcd for $C_{23}H_{18}N_5Br$ 443.0745, found 443.0792.

5.13. 7-Biphenyl-4-ylmethyl-N^4-(3-bromo-phenyl)-7*H*-pyrrolo [2,3-*d*]pyrimidine-2,4-diamine (18a)

Reaction of **29** (500 mg, 1.64 mmol), **30j** (666 mg, 3.28 mmol) and sodium hydride (37 mg, 1.55 mmol), using the general procedure described above, gave **18a**: yield 10%, mp 86.2 °C; TLC R_f 0.82 ($CHCl_3/CH_3OH$, 10:1 with two drops concentrated NH_4OH); ^1H NMR (DMSO-d_6): δ 5.24 (s, 2H, CH_2), 5.99 (br s, 2H, NH_2, exch), 6.64 (s, 1H, C5–CH), 6.91 (s, 1H, C6–CH), 7.07–8.11 (m, 13H, Ar–H), 9.12 (s, 1H, NH, exch). HRMS calcd for $C_{25}H_{20}N_5Br$ 469.0902, found 469.1001.

5.14. N^4-(3-Bromo-phenyl)-7-(3,4,5-trimethoxy-benzyl)-7*H*-pyrrolo[2,3-*d*]pyrimidine-2,4-diamine (19a)

Reaction of **29** (400 mg, 1.31 mmol), **30k** (570 mg, 2.63 mmol) and sodium hydride (31 mg, 1.31 mmol), using the general procedure described above, gave **19a**: yield 14%, mp 113.6 °C; ^1H NMR (DMSO-d_6): δ 3.61 (s, 3H, OCH_3), 3.69 (s, 6H, 2 × OCH_3), 5.10 (s, 2H, CH_2), 5.99 (br s, 2H, NH_2, exch), 6.60 (s, 1H, C5–CH), 6.60 (s, 2H, Ar–H), 6.90 (s, 1H, C6–CH), 7.12–8.12 (m, 4H, Ar–H), 9.09 (s, 1H, NH, exch). TLC R_f 0.85 ($CHCl_3/CH_3OH$, 10:1 with two drops concentrated NH_4OH); Anal. ($C_{22}H_{22}N_5BrO_3$) C, H, N, Br.

5.15. 4-Chloro-7-(2-chlorobenzyl)-7*H*-pyrrolo[2,3-*d*]pyrimidin-2-amine (31)

To a round bottomed flask was added **27** (60 mg, 0.35 mmol) and dissolved in 5 ml of DMF. The solution was cooled to 0 °C and sodium hydride (9 mg, 0.33 mmol) was added. After stirring at 0 °C for 1 h **30c** (81 mg, 0.39 mmol) was added. The reaction was continued at rt for 2 h, at the end of which the reaction was quenched with water. The water phase was extracted with ethylacetate. The organic phase was dried over sodium sulfate and evaporated under reduced pressure. The residue was dissolved in methylene chloride, 250 mg silica gel was added to the solution which was then evaporated to dryness to form a plug. The silica gel plug obtained was loaded onto a silica gel column and eluted with 4:1 hexane/ethylacetate. Fractions corresponding to the product (TLC) were pooled and evaporated to dryness under reduced pressure to afford the product **31** as a white solid: yield 48%, mp 148 °C; TLC R_f 0.23 (hexane/EtOAc, 4:1); ^1H NMR (DMSO-d_6): δ 5.32 (s, 2H, CH_2), 6.39 (d, J = 4 Hz, 1H, C5–CH), 6.65–6.73 (bs, 2H, NH_2, exch), 6.71 (d, J = 16 Hz, 1H, Ar-H), 7.17–7.18 (d, 1H, C6–CH), 7.22–7.50 (m, 4H, Ar–H). Anal. ($C_{13}H_{10}Cl_2N_4$) C, H, N, Cl.

6. Molecular modeling and computational studies

The X-ray crystal structure of VEGFR2 at 1.71 Å resolution was obtained from the protein database (PDB ID 1YWN).[38] This crystal structure contains VEGFR2 in complex with a novel 4-aminofuro[2,3-*d*]pyrimidine. Docking studies were performed using the docking suite of Molecular Operating Environment software (MOE 2008.10)[37] and Flexx 3.1.2.[45] After addition of hydrogen atoms, the protein was then 'prepared' using the LigX function in MOE. LigX is a graphical interface and collection of procedures for conducting interactive ligand modification and energy minimization in the active site of a flexible receptor. In LigX calculations, the receptor atoms far from the ligand are constrained and not allowed to move while receptor atoms in the active site of the protein are allowed to move but are subject to tether restraints that discourage gross movement.[37] This procedure was performed with the default settings. Ligands were built using the molecule builder function in MOE and were energy minimized to its local minima using the MMF94X forcefield to a constant of 0.05 kcal/mol. Ligands were docked into the active site of the prepared protein using the docking suite as implemented in MOE. The docking was restricted to the active site pocket residues using Alpha triangle placement method. Refinement of the docked poses was carried out using the Forcefield refinement scheme and scored using Affinity dG scoring system. Around 30 poses were returned for each compound at the end of each docking run. The docked poses were manually examined in the binding pocket to ensure quality of docking and to confirm absence of steric clashes with the amino acid residues of the binding pocket.

To validate the utility of MOE 2008.10 for docking ligands into the active site, the native ligand in the crystal structure (PDB: 1YWN) was built using the molecule builder, energy minimized using MMFF94x forcefield to a gradient of 0.05 kcal/mol and docked into the active site using the above parameters. The best docked pose of the native ligand displayed an RMSD of 0.6031 Å compared to the crystal structure pose. MOE 2008.10 was thus validated for our docking process.

Docking with Flexx 3.1.2 was carried out in by defining the active site as a sphere of ~6.5 Å from the ligand. The protonation states utilized for the proteins and the ligands were calculated using the default settings. Water molecules in the active site were permitted to rotate freely. Ligands for docking were prepared using MOE and energy minimized using the MMF94X forcefield to a constant of 0.05 kcal/mol. Triangle matching was used as the placement method and the docked poses were scored using default settings. The docked poses were exported and visualized in MOE. The best docked pose had an RMSD of 0.7686 Å. Flexx 3.1.2 was thus validated for our docking process.

Docking studies were performed for **11** and **11a** in MOE and Flexx using a similar procedure. Poses from the docking experiment performed in Flexx were exported and visualized in MOE.

6.1. Cells

All cells were maintained at 37 °C in a humidified environment containing 5% CO_2 using media from Mediatech (Hemden, NJ). A-431 cells were from the American Type Tissue Collection (Manassas, VA).

6.2. Chemicals

All growth factors (bFGF, VEGF, EGF, and PDGF-β) were purchased from Peprotech (Rocky Hill, NJ). PD153035, SU5416, AG1295, and CB676475 (4-[(4′-chloro-2′-fluoro)phenylamino]-6,7-dimethoxyquinazoline) were purchased from Calbiochem (San Diego, CA). The CYQUANT cell proliferation assay was from Molecular Probes (Eugene, OR). All other chemicals were from Sigma Chemical unless otherwise noted.

6.3. Antibodies

The PY-HRP antibody was from BD Transduction Laboratories (Franklin Lakes, NJ). Antibodies against EGFR, PDGFR-β, FGFR-1, Flk-1, and Flt-1 were purchased from Upstate Biotech (Framingham, MA).

6.4. Phosphotyrosine ELISA

Cells used were tumor cell lines naturally expressing high levels of EGFR (A431), Flk-1 (U251), Flt-1 (A498), PDGFR-β (SF-539), and FGFR-1 (NIH OVCAR-8). Expression levels at the RNA level were derived from the NCI Developmental Therapeutics Program (NCI-DTP) web site public molecular target information (http://www.dtp.nci.nih.gov/mtargets/mt_index.html). Briefly, cells at 60–75% confluence were placed in serum-free medium for 18 h to reduce the background of phosphorylation. Cells were always >98% viable by Trypan blue exclusion. Cells were then pretreated for 60 min with 10, 3.33, 1.11, 0.37, and 0.12 μM compounds followed by 100 ng/ml EGF, VEGF, PDGF-BB, or bFGF for 10 min. The reaction was stopped and cells permeabilized by quickly removing the media from the cells and adding ice-cold Tris-buffered saline (TBS) containing 0.05% Triton X-100, protease inhibitor cocktail, and tyrosine phosphatase inhibitor cocktail. The TBS solution was then removed and cells fixed to the plate for 30 min at 60 °C and further incubation in 70% ethanol for an additional 30 min. Cells were further exposed to block (TBS with 1% BSA) for 1 h, washed, and then a horseradish peroxidase (HRP)-conjugated phosphotyrosine (PY) antibody added overnight. The antibody was removed, cells were washed again in TBS, exposed to an enhanced luminal ELISA substrate (Pierce Chemical, Rockford, IL), and light emission measured using a UV product (Upland, CA) BioChemi digital darkroom. The known RTK-specific kinase inhibitor, PD153035, was used as a positive control compound for EGFR kinase inhibition; SU5416 for Flk-1 kinase inhibition; AG1295 for PDGFR-β kinase inhibition; and CB676475 (4-[(4′-chloro-2′-fluoro)phenylamino]-6,7-dimethoxyquinazoline) was used as a positive control for both Flt-1 and Flk-1 kinase inhibition. Data were graphed as a percent of cells receiving growth factor alone and IC_{50} values were estimated from two to three separate experiments (n = 8–24) using hand-drawn probit plots. In each case, the activity of a positive control inhibitor did not deviate more than 10% from the IC_{50} values listed in the text.

6.5. CYQUANT cell proliferation assay

As a measure of cell proliferation, the CYQUANT cell counting/proliferation assay was used as previously described.[35] Briefly, cells are first treated with compounds for 12 h and then allowed to grow for an additional 36 h. The cells are then lysed and the CYQUANT dye, which intercalates into the DNA of cells, is added and after 5 min the fluorescence of each well measured using a UV product BioChemi digital darkroom. A positive control used for cytotoxicity in each experiment was cisplatin, with an apparent average IC_{50} value of 8.2 ± 0.65 μM. Data are graphed as a percent of cells receiving growth factor alone and IC_{50} values estimated from two to three separate experiments (n = 6–15) using probit plots.

6.6. Statistics

All analysis was done using Prism 4.0. (GraphPad Software, San Diego, CA).

6.7. Whole animal toxicity assay

To first determine the maximal tolerated dose (MTD) of a drug, groups of four male NCr nu/nu mice at 8 weeks of age without tumors were injected with 5, 10, 15, 25, 35, and 45 mg/kg **11a** and 5, 10, 15 and 20 mg/kg **8** three times weekly on Monday AM, Wednesday noon and Friday PM. Weights were taken and animals observed for acute distress during the first 96 h after injection. No apparent toxicity and no significant weight loss (P >0.05; one-way ANOVA with Repeated Measures Post-Test) was observed throughout a 6 week period after drug administration.

6.8. COLO-205. human metastatic colon mouse xenograft

One million COLO-205 (liver colonizing; American Type Culture Collection) human metastatic colon cancer cells were injected SQ into the lateral flank of athymic NIH-II male mice, 8 weeks in age. Animals are monitored every other day for the presence of tumors. At the time in which most tumors are measurable by calipers (days 8–11 after implantation), animals with tumors are randomly sorted into treatment groups. DMSO stocks (30 mM) of drugs are further dissolved into sterile water for injection and the optimal dose (from MTD studies) injected intraperitoneally (IP). The length (long side), width (short side) and depth of the tumors were measured using digital Vernier Calipers each Monday, Wednesday, and Friday. Tumor volume is calculated using the formula length $\times$ width $\times$ depth. Tumor growth rate is calculated using a linear regression analysis algorithm with the software GraphPad Prism 4.0.c (GraphPad software, San Diego, CA). At the experiment's end, animals were humanly euthanized using carbon dioxide, tumors and liver excised, fixed in 20% neutral buffered formalin for 8–10 h, embedded into paraffin, and hematoxylin-eosin (H&E) stain of 3–4 separate tissue sections completed to span the tumor/liver. Together with the OUHSC Department of Pathology core, metastases per liver lobe were counted using the H&E stained sections. The metastases could be seen as purple clusters of disorganized cells on the highly organized largely pink liver. Together with the OUHSC Department of Pathology core, blood vessels per unit area on primary tumors are also counted in 5 fields at 100x magnification and averaged.

Acknowledgments

This work was supported, in part, by the National Institutes of Health and National Cancer Institute Grant CA98850 (A.G.) and the Duquesne University Adrian Van Kaam Chair in Scholarly Excellence (AG).

Supplementary data

Supplementary data (elemental analysis and high-resolution mass spectra (HRMS) (ESI)) associated with this article can be found, in the online version, at doi:10.1016/j.bmc.2012.01.029.

References and notes

1. Johnson, G. L.; Lapadat, R. *Science (Washington, DC, U.S.)* **2002**, *298*, 1911.
2. Blume-Jensen, P.; Hunter, T. *Nature (London, U. K.)* **2001**, *411*, 355.
3. Quesada, A. R.; Munoz-Chapuli, R.; Medina, M. A. *Med. Res. Rev.* **2006**, *26*, 483.
4. Holmgren, L.; O'Reilly, M. S.; Folkman, J. *Nat. Med.* **1995**, *1*, 149.
5. Fukumura, D.; Xu, L.; Chen, Y.; Gohongi, T.; Seed, B.; Jain, R. K. *Cancer Res.* **2001**, *61*, 6020.
6. Dvorak, H. F. *J. Clin. Oncol.* **2002**, *20*, 4368.
7. Carmeliet, P. *Nat. Med. (New York, NY, United States)* **2003**, *9*, 653.
8. Gschwind, A.; Fischer, O. M.; Ullrich, A. *Nat. Rev. Cancer* **2004**, *4*, 361.
9. Board, R.; Jayson, G. C. *Drug Resist. Updates* **2005**, *8*, 75.
10. Eskens, F. A. L. M. *Brit. J. Cancer* **2004**, *90*, 1.
11. Vieth, M.; Sutherland, J. J.; Robertson, D. H.; Campbell, R. M. *Drug Discovery Today* **2005**, *10*, 839.
12. Comis, R. L. *Oncologist* **2005**, *10*, 467.
13. Faivre, S.; Djelloul, S.; Raymond, E. *Semin. Oncol.* **2006**, *33*, 407.
14. Tabernero, J. *Mol. Cancer Res.* **2007**, *5*, 203.
15. Hicklin, D. J.; Ellis, L. M. *J. Clin. Oncol.* **2005**, *23*, 1011.
16. Klebl, B. M.; Mueller, G. *Expert Opin. Ther. Targets* **2005**, *9*, 975.
17. Marcucci, G.; Perrotti, D.; Caligiuri, M. A. *Clin. Cancer Res.* **2003**, *9*, 1248.
18. Chow, L. Q. M.; Eckhardt, S. G. *J. Clin. Oncol.* **2007**, *25*, 884.
19. Gridelli, C.; Maione, P.; Del Gaizo, F.; Colantuoni, G.; Guerriero, C.; Ferrara, C.; Nicolella, D.; Comunale, D.; De Vita, A.; Rossi, A. *Oncologist* **2007**, *12*, 191.
20. Nelson, M. H.; Dolder, C. R. *Ann. Pharmacother.* **2006**, *40*, 261.
21. Erber, R.; Thurnher, A.; Katsen, A. D.; Groth, G.; Kerger, H.; Hammes, H.-P.; Menger, M. D.; Ullrich, A.; Vajkoczy, P. *FASEB J.* **2004**, *18*, 338.
22. Timke, C.; Zieher, H.; Roth, A.; Hauser, K.; Lipson, K. E.; Weber, K. J.; Debus, J.; Abdollahi, A.; Huber, P. E. *Clin. Cancer Res.* **2008**, *14*, 2210.
23. Hoekman, K. *Cancer J.* **2001**, S134.
24. Laird, A. D.; Vajkoczy, P.; Shawver, L. K.; Thurnher, A.; Liang, C.; Mohammadi, M.; Schlessinger, J.; Ullrich, A.; Hubbard, S. R.; Blake, R. A.; Fong, T. A.; Strawn, L. M.; Sun, L.; Tang, C.; Hawtin, R.; Tang, F.; Shenoy, N.; Hirth, K. P.; McMahon, G. *Cancer Res.* **2000**, *60*, 4152.
25. Gangjee, A.; Yang, J.; Ihnat, M. A.; Kamat, S. *Bioorg. Med. Chem.* **2003**, *11*, 5155.
26. Schilder, R. J.; Hall, L.; Monks, A.; Handel, L. M.; Fornace, A. J., Jr.; Ozols, R. F.; Fojo, A. T.; Hamilton, T. C. *Int. J. Cancer* **1990**, *45*, 416.
27. Gangjee, A.; Yu, J.; Kisliuk, R. L. *J. Heterocycl. Chem.* **2002**, *39*, 833.
28. Gangjee, A.; Brian, K. Unpublished work.
29. Fong, T. A. T.; Shawver, L. K.; Sun, L.; Tang, C.; App, H.; Powell, T. J.; Kim, Y. H.; Schreck, R.; Wang, X.; Risau, W.; Ullrich, A.; Hirth, K. P.; McMahon, G. *Cancer Res.* **1999**, *59*, 99.
30. Stockwell, B. R.; Haggarty, S. J.; Schreiber, S. L. *Chem. Biol.* **1999**, *6*, 71.
31. Smith, G. K.; Wood, E. R. *Drug Discovery Today: Technol.* **2010**, *7*, e13.
32. Falgueyret, J.-P.; Black, W. C.; Cromlish, W.; Desmarais, S.; Lamontagne, S.; Mellon, C.; Riendeau, D.; Rodan, S.; Tawa, P.; Wesolowski, G.; Bass, K. E.; Venkatraman, S.; Percival, M. D. *Anal. Biochem.* **2004**, *335*, 218.
33. Weissman, A.; Keefer, J.; Miagkov, A.; Sathyamoorthy, M.; Perschke, S.; Wang, F. L. In *Comprehensive Medicinal Chemistry II*; John, B. T., David, J. T., Eds.; Elsevier: Oxford, 2007; p 617.
34. Zeng, X.-F.; Li, W.-W.; Fan, H.-J.; Wang, X.-Y.; Ji, P.; Wang, Z.-R.; Ma, S.; Li, L.-L.; Ma, X.-F.; Yang, S.-Y. *Bioorg. Med. Chem. Lett.* **2011**, *21*, 4742.
35. Wilson, S. M.; Barsoum, M. J.; Wilson, B. W.; Pappone, P. A. *Cell Prolif.* **1999**, *32*, 131.
36. Rarey, M.; Kramer, B.; Lengauer, T.; Klebe, G. *J. Mol. Biol.* **1996**, *261*, 470.
37. Molecular Operating environment (MOE 2008.10), C. C. G., Inc., 1255 University Street, Suite 1600, Montreal, Quebec, Canada, H3B 3X3. www.chemcomp.com.
38. Miyazaki, Y.; Matsunaga, S.; Tang, J.; Maeda, Y.; Nakano, M.; Philippe, R. J.; Shibahara, M.; Liu, W.; Sato, H.; Wang, L.; Nolte, R. T. *Bioorg. Med. Chem. Lett.* **2005**, *15*, 2203.
39. Gangjee, A.; Zaware, N.; Raghavan, S.; Ihnat, M.; Shenoy, S.; Kisliuk, R. L. *J. Med. Chem.* **2010**, *53*, 1563.
40. Traxler, P. M.; Furet, P.; Mett, H.; Buchdunger, E.; Meyer, T.; Lydon, N. *J. Med. Chem.* **1996**, *39*, 2285.
41. Laufer, S. A.; Domeyer, D. M.; Scior, T. R. F.; Albrecht, W.; Hauser, D. R. J. *J. Med. Chem.* **2005**, *48*, 710.
42. Choowongkomon, K.; Sawatdichaikul, O.; Songtawee, N.; Limtrakul, J. *Molecules* **2010**, *15*, 4041.
43. Schroeder, M. C.; Hamby, J. M.; Connolly, C. J. C.; Grohar, P. J.; Winters, R. T.; Barvian, M. R.; Moore, C. W.; Boushelle, S. L.; Crean, S. M.; Kraker, A. J.; Driscoll, D. L.; Vincent, P. W.; Elliott, W. L.; Lu, G. H.; Batley, B. L.; Dahring, T. K.; Major, T. C.; Panek, R. L.; Doherty, A. M.; Showalter, H. D. H. *J. Med. Chem.* **1915**, *2001*, 44.
44. Shaheen, R. M.; Davis, D. W.; Liu, W.; Zebrowski, B. K.; Wilson, M. R.; Bucana, C. D.; McConkey, D. J.; McMahon, G.; Ellis, L. M. *Cancer Res.* **1999**, *59*, 5412.
45. Flexx, 3.1.2 BioSolveIT GmbH.